Journal of Energy Chemistry 27 (2018) 472–477

Contents lists available at ScienceDirect

Journal of Energy Chemistry

journal homepage: www.elsevier.com/locate/jechem

http://www.journals.elsevier.com/journal-of-energy-chemistry/

One-step synthesis of graphitic-C_3N_4/ZnS composites for enhanced supercapacitor performance

Binbin Wei[a], Hanfeng Liang[b,*], Rongrong Wang[a], Dongfang Zhang[a], Zhengbing Qi[c], Zhoucheng Wang[a,**]

[a] College of Chemistry and Chemical Engineering, Xiamen University, Xiamen 361005, Fujian, China
[b] Materials Science and Engineering, King Abdullah University of Science and Technology (KAUST), Thuwal 23955, Saudi Arabia
[c] School of Materials Science and Engineering, Xiamen University of Technology, Xiamen 361024, Fujian, China

ARTICLE INFO

Article history:
Received 6 September 2017
Revised 3 November 2017
Accepted 19 November 2017
Available online 23 November 2017

Keywords:
g-C_3N_4/ZnS
Supercapacitor
One-step calcination
Energy storage

ABSTRACT

A series of graphitic-C_3N_4/ZnS (g-C_3N_4/ZnS) supercapacitor electrode materials have been prepared via a one-step calcination process of zinc acetate/thiourea with different mass ratios under nitrogen atmosphere. The optimized g-C_3N_4/ZnS composite shows a highest specific capacitance of 497.7 F/g at 1 A/g and good cycling stability with capacitance retention of 80.4% at 5 A/g after 1000 cycles. Moreover, g-C_3N_4/ZnS composites display an improved supercapacitor performance in terms of specific capacitance compared to the pure g-C_3N_4 and ZnS. In addition, our designed symmetric supercapacitor device based on g-C_3N_4/ZnS composite electrodes can exhibit an energy density of 10.4 Wh/kg at a power density of 187.3 W/kg. As a result, g-C_3N_4/ZnS composites are expected to be a prospective material for supercapacitors and other energy storage applications.

1. Introduction

Supercapacitors as energy storage devices exhibit better cycling performance, faster charge-discharge rate and higher power density than existing batteries and traditional capacitors, thus attracting great attention in recent years [1–4]. Generally, there are two classes of supercapacitors based on the different charge storage mechanism: electrical double layer capacitors (EDLCs) and pseudocapacitors [2]. Carbon-based materials are employed as electrode materials for EDLCs [5]. However, the specific capacitance is usually very low [6]. Meanwhile, transition metal oxides and hydroxides used for pseudocapacitors suffer from low specific power density [7–9]. In recent years, metal sulfides have aroused more interest from researchers toward their applications as electrode materials for pseudocapacitors due to their two or more valence states and high theoretical capacity [10–12]. Among these, zinc sulfide (ZnS) has been widely used in energy storage devices because of its advantages of good electrical conductivity, electronic properties and stability [13–15]. Nonetheless, ZnS-based electrode materials still suffer from relatively low specific capacitance. A good way to solve the as-mentioned issue is to design the hybrid electrode with a combination of carbon-based materials and pseudocapacitive materials. Compared to single-phase electrode material, the composite structure can improve the supercapacitor performance [16]. The g-C_3N_4 carbon materials with excellent mechanical strength and thermal conductivity show good performance in many fields such as wastewater detoxification [17], H_2 production [18], fuel cells [19], and supercapacitors [20]. To the best of our knowledge, g-C_3N_4/ZnS composites have been widely investigated in the photocatalytic field [21–23]. However, no reports about the supercapacitor performance studies of g-C_3N_4/ZnS composites have been recorded.

In the current work, g-C_3N_4/ZnS composites have been synthesized via a facile calcination method and their applications for supercapacitors are investigated for the first time. With an optimal composition, the as-prepared g-C_3N_4/ZnS composites show much better electrochemical performance with a specific capacitance of 497.7 F/g at 1 A/g than the pristine g-C_3N_4 and ZnS, respectively. More importantly, the symmetric g-C_3N_4/ZnS//g-C_3N_4/ZnS supercapacitor device can achieve an energy density of 10.4 Wh/kg at a power density of 187.3 W/kg.

* Corresponding author.
** Corresponding author.
E-mail addresses: hanfeng.liang@kaust.edu.sa (H. Liang), zcwang@xmu.edu.cn (Z. Wang).

https://doi.org/10.1016/j.jechem.2017.11.015

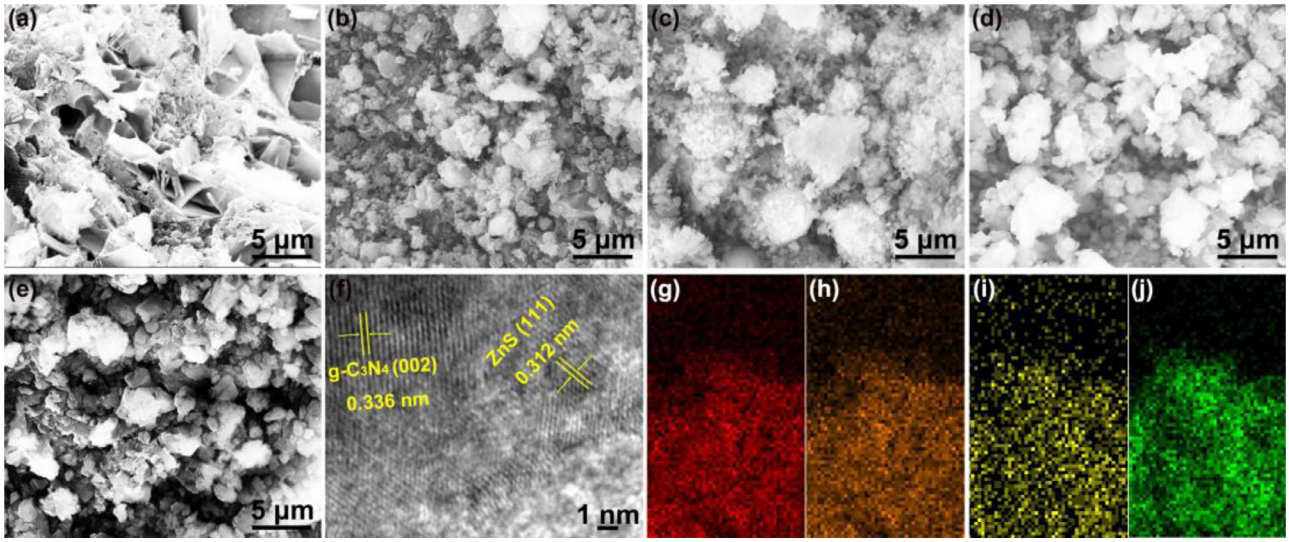

Fig. 1. SEM images of (a) ZT0, (b) ZT0.005, (c) ZT0.02, (d) ZT0.05 and (e) ZT0.1 composites. (f) HRTEM image and HRTEM mapping of (g) C element, (h) N element, (i) S element and (j) Zn element of the ZT0.02 composite.

2. Experimental

2.1. Synthesis of g-C_3N_4/ZnS composites

A specific amount of zinc acetate (0.005, 0.02, 0.05 and 0.1 g) and 1 g of thiourea were ground sufficiently and then annealed at 500 °C for 2 h in the tube furnace at a ramp rate of 10 °C/min under a nitrogen atmosphere. After being cooled down to room temperature, the yellow powder was obtained. Based on different mass ratios of zinc acetate/thiourea in the reactants, the final samples were labeled as ZT*x*, where *x* are 0.005, 0.02, 0.05 and 0.1, respectively. For comparison, the pure g-C_3N_4 (denoted as ZT0) was also synthesized under the same condition without the addition of zinc acetate. In addition, the nanostructured ZnS (denoted as ZS) was prepared according to the previously reported method for electrochemical performance comparison [21].

2.2. Fabrication of electrodes

The active materials (as-prepared samples), polyvinylidene fluoride (PVDF) and carbon black were mixed in a mass ratio of 75:15:10 in *N*-methylpyrrolidone (NMP) solvent to form a slurry. Afterward, the slurry was coated onto the nickel foam (2 cm × 1 cm) and then dried at 40 °C for 12 h in a vacuum oven. The mass loading of active materials is ~2.7 mg/cm^2.

2.3. Characterizations

The morphological studies were carried out using scanning electron microscopy (SEM, ZEISS Sigma). X-ray diffraction (XRD, Rigaku Ultima IV) with Cu-*Kα* radiation source ($\lambda = 1.541$ Å) was used to identify the phase structure of the prepared composites. The chemical bonding states of the composites were analyzed by X-ray photoelectron spectroscopy (XPS, PHI QUANTUM 2000). The BET surface area measurements were done by N_2 adsorption–desorption method at 77 K using Micromeritics Tristar-3020.

2.4. Electrochemical measurements

The electrochemical performance was tested in 6 M KOH aqueous solution using both a conventional three-electrode and two-electrode configurations. For the three-electrode system, the electrode prepared above, platinum foil and Hg/HgO electrode were used as the working, counter and reference electrodes, respectively. For the two-electrode system, two identical g-C_3N_4/ZnS composite electrodes were used to assemble a symmetric supercapacitor device with polymer filtering membrane (Celgrad 3501) as the separator. Cyclic voltammetry (CV), galvanostatic charge-discharge (GCD) and electrochemical impedance spectroscopy (EIS) tests were conducted on a CHI660E electrochemical station (Chenhua Corp. Shanghai). The EIS tests were performed over the frequency range from 0.01 to 100,000 Hz at the open circuit potential with an AC voltage of 5 mV. The specific capacitance (C_s, F/g) for single electrode was calculated according to the following equation [24]:

$$C_s = 21 \int V dt / \left(m \cdot V^2 \Big|_{Vi}^{Vf} \right) \quad (1)$$

whereas for the symmetric supercapacitor device, the cell capacitance (C_{cell}, F/g) was calculated based on

$$C_{cell} = 21 \int V dt / \left(M \cdot V^2 \Big|_{Vi}^{Vf} \right) \quad (2)$$

where I (A) is the constant current, t (s) is the discharge time, V (V) is the total potential difference with initial and final values of V_i and V_f, respectively, m (g) is the weight of active materials for single electrode, and M (g) is the weight of active materials for both two electrodes. The energy density (E, Wh/kg) and power density (P, W/kg) were estimated by:

$$E = C_{cell} \times V^2 / (2 \times 3.6) \quad (3)$$

$$P = (3600 \cdot E)/t \quad (4)$$

3. Results and discussion

Fig. 1(a–e) shows the SEM micrographs of g-C_3N_4/ZnS composites. A sheet-like structure similar to graphene can be observed from sample ZT0. However, all composites containing ZnS show spherical agglomerate clusters. Meanwhile, a large number of gaps between clusters can be noted, which can achieve a high specific surface area and provide a channel for the movement of electrolyte ions. The HRTEM image of the ZT0.02 composite is shown in Fig. 1(f). In comparison to the data in JCPDS, the lattice fringes

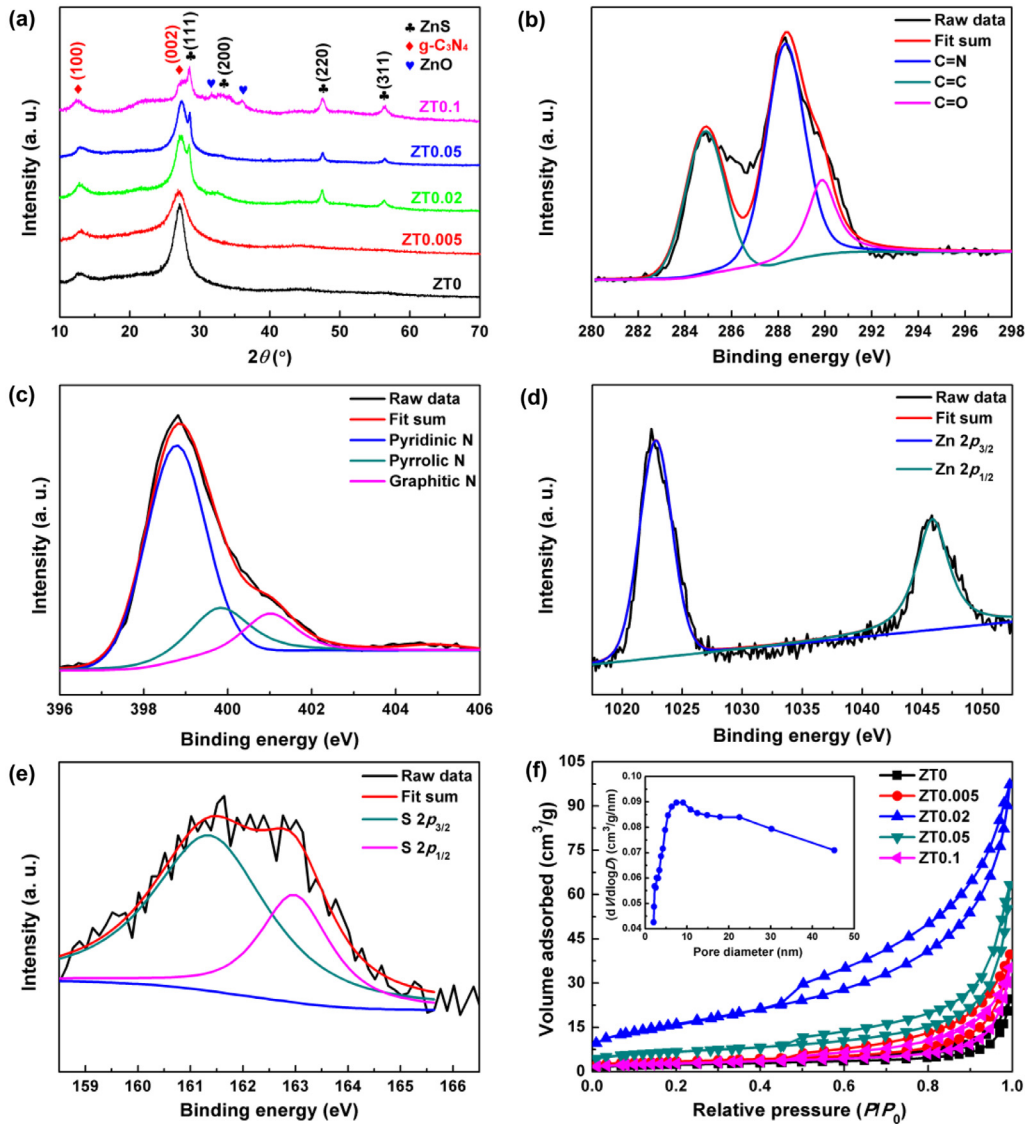

Fig. 2. (a) XRD patterns of the g-C_3N_4/ZnS compositions. (b) C 1*s*, (c) N 1*s*, (d) Zn 2*p* and (e) S 2*p* XPS spectra of ZT0.02 composite. (f) The N_2 adsorption–desorption isotherms of the g-C_3N_4/ZnS compositions (the inset shows the BJH pore size distribution of ZT0.02 composite).

with a spacing of 0.336 nm and 0.312 nm belong to the (002) plane of g-C_3N_4 (JCPDS No. 87-1526) and the (111) plane of cubic ZnS (JCPDS No. 05-0566), respectively, which can be further corroborated by XRD. To further confirm the presence and dispersion state of elements in the g-C_3N_4/ZnS composites, HRTEM mapping was performed, and the results are shown in Fig. 1(g–j). It is evident that C, N, S and Zn elements are visible and well-dispersed distributions.

Fig. 2(a) presents the XRD patterns of all the composite samples. The strong peak at 27.5° and the weak peak at 13.1° correspond to the (002) and (100) planes of g-C_3N_4 (JCPDS No. 87-1526), respectively [25]. However, the characteristic diffraction peaks of ZnS cannot be observed from the composite samples ZT0 and ZT0.005. With the further increase in the mass ratio up to 0.02 and above, four additional diffraction peaks at around 28.5°, 33.1°, 47.5°, and 56.3° are found to match well to the (111), (200), (220), and (311) planes of cubic ZnS (JCPDS No. 05-0566) [14]. As shown in Fig. 2(a), a shift from g-C_3N_4 to g-C_3N_4/ZnS is clearly seen with increasing mass ratio of zinc acetate/thiourea, demonstrating the formation of g-C_3N_4/ZnS composites. The absence of any other impurity peaks exhibits no other crystalline impurity phase (ZT0.02 and ZT0.05). Nevertheless, for the ZnS rich composite ZT0.1, the impurity peaks indexed to ZnO are observed because of the oxidation of ZnS.

In order to investigate the chemical bonding states of g-C_3N_4/ZnS composites, all the composites were characterized by XPS technique and only the XPS spectrum of a representative sample ZT0.02 is shown. As depicted in Fig. 2(b), the primary peaks at 284.6 and 289.9 eV are ascribed to the C=C and C=O components of the atmosphere, respectively. In addition, the peak at 288.6 eV can be assigned to the C–N bonds of g-C_3N_4 [26]. The peaks at 398.6, 400.2, and 401.3 eV in Fig. 2(c) correspond to three different types of chemical states of N 1*s*, manifesting the existence of C–N=C, (N–(C)$_3$), and C–N–H groups, respectively [27]. Fig. 2(d) shows the presence of Zn $2p_{1/2}$ and Zn $2p_{3/2}$ components that have binding energies of 1045.6 and 1022.7 eV, respectively [28]. In Fig. 2(e), the S $2p_{3/2}$ (161.4 eV) and S $2p_{1/2}$ (162.8 eV) lines indicate the existence of S^{2-} [29]. The XPS results again confirm the formation of g-C_3N_4/ZnS composites, which is in good agreement with the XRD results.

Fig. 2(f) displays the N_2 adsorption–desorption isotherms of g-C_3N_4/ZnS compositions. The N_2 adsorption–desorption isotherms

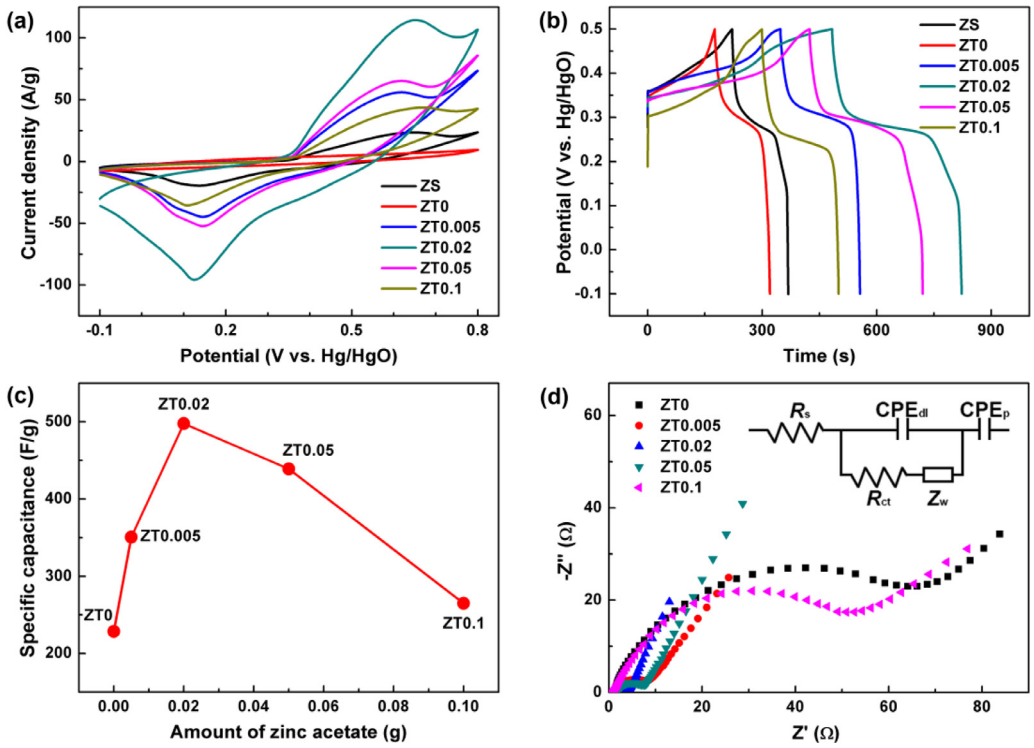

Fig. 3. (a) CV curves at a scan rate of 100 mV/s, (b) GCD curves at a current density of 1 A/g, (c) comparison of specific capacitances at a current density of 1 A/g, and (d) EIS analysis (the inset shows the corresponding equivalent circuit model) of the composite electrodes.

Table 1. Specific surface areas of the g-C_3N_4/ZnS compositions.

Sample	ZT0	ZT0.005	ZT0.02	ZT0.05	ZT0.1
Specific surface area (m^2/g)	9	12	59	24	10

of all composite samples are classified as type IV with an H3-type hysteresis loop in the relative pressure range from 0.45 to 1.0, which is an adsorption–desorption characteristic of mesoporous materials (2–50 nm). The BJH pore size distribution of the ZT0.02 sample (inset of Fig. 2f) further confirms the mesoporous structure. The formation of porous structure is ascribed to the aggregation of g-C_3N_4/ZnS composites. The specific surface areas of all composite samples are shown in Table 1. The ZT0.02 sample possesses a higher specific surface area of 59 m^2/g than other composites. It is believed that a large specific surface area is beneficial to improve the supercapacitor performance [30,31].

To evaluate the electrochemical performance of the composite electrodes, all the electrochemical tests were carried out in a typical three-electrode system. Fig. 3(a) illustrates the CV curves of the composite electrodes at a scan rate of 100 mV/s in a potential range from −0.1 to 0.8 V (versus Hg/HgO). The CV curve of the ZT0 sample (pure g-C_3N_4) presents a typical quasi-rectangular shape without redox peaks, which is in consistent with the literature reported [20]. However, a couple of obvious redox peaks similar to pure ZnS appear upon the addition of zinc acetate, showing a pseudocapacitive behavior. Therefore, the redox peaks can be explained by the valence state conversion between ZnS and ZnSO as proposed by Pu et al. [32]. Moreover, the integrated areas under the CV curves increase with the incorporation of more ZnS when the mass ratio of zinc acetate/thiourea is less than 0.02. However, the further increase of zinc acetate content leads to a decrease of the integral area. The same trend is also observed in specific capacitance because it is proportional to the integrated area of CV curves [33]. The GCD curves of the composite electrodes at a current density of 1 A/g are shown in Fig. 3(b). It is noted that the ZT 0.02 composite electrode shows the longest discharge time, again confirming the superior electrochemical performance. Furthermore, the voltage drop of the ZT0.02 composite electrode is about 0.12 V, implying a small internal resistance [34]. The specific capacitances are summarized and compared in Fig. 3(c). Notably, the ZT0.02 composite electrode exhibits the highest specific capacitance of 497.7 F/g at 1 A/g, which is in accordance with the CV evaluation. The enhancement in specific capacitance can be attributed to the porous structure and the higher specific surface area, which can not only promote the fast diffusion of ions from the electrolyte to the electrode, but also can provide more active sites for redox reactions. The EIS of the composite electrodes was measured and the Nyquist plots are shown in Fig. 3(d). The inset shows the corresponding equivalent circuit model. As shown in Fig. 3(d), the ZT0.02 composite electrode shows the lowest charge-transfer impedance, indicating a fast charge transfer process for the electrons and ions into the inlayer of active materials [35], which guarantees excellent rate performance. Clearly, ZT0.02 composite electrode shows better capacitive performance than others due to the nearly vertical slope at the low frequency section [36].

The ZT0.02 composite electrode is selected as a representative candidate for further electrochemical investigation. Fig. 4(a) shows the CV curves of the ZT0.02 composite electrode at various scan rates of 10–100 mV/s. The redox peaks still exist even at a scan rate of 100 mV/s, suggesting good reaction reversibility and outstanding rate performance. The GCD curves of the ZT0.02 composite electrode at different current densities are shown in Fig. 4(b). All the GCD curves show the obvious discharge plateaus, further demonstrating the pseudocapacitive behaviour [35]. The specific capacitances of the ZT0.02 composite electrode derived from the discharge curves are shown in Fig. 4(c). The specific capacitances for the ZT0.02 composite electrode are 497.7, 466.8, 401.5 and 349.7 F/g at 1, 2, 5 and 10 A/g, respectively, which is much

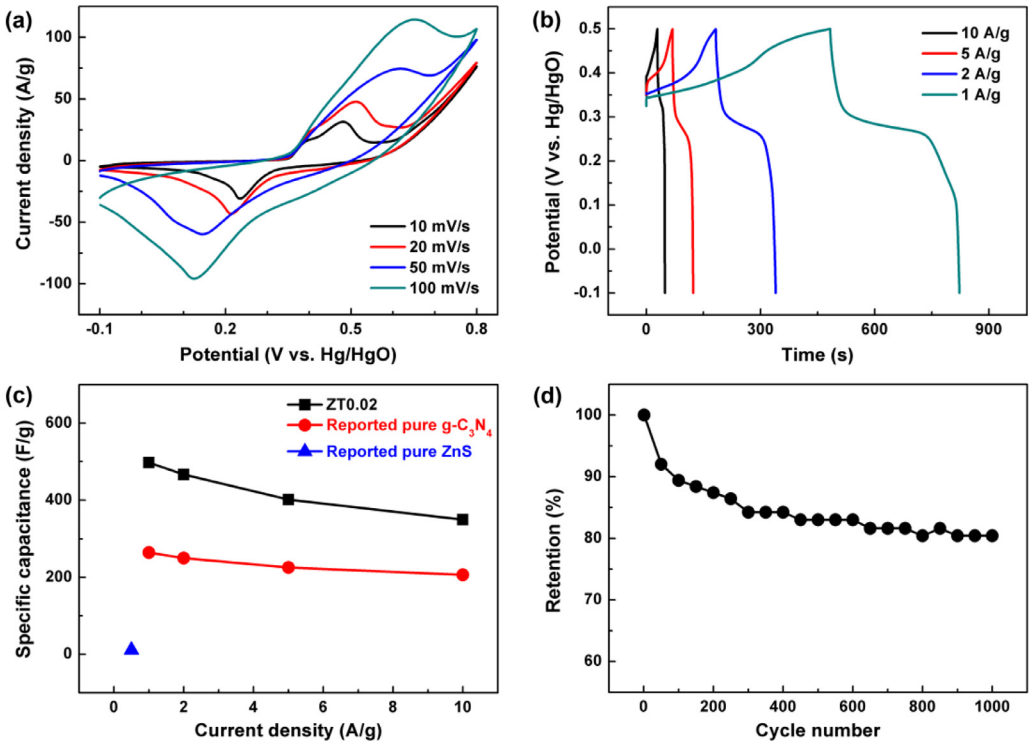

Fig. 4. (a) CV curves at different scan rates, (b) GCD curves at different current densities, (c) comparison of specific capacitances at different current densities, and (d) cycling stability at a current density of 5 A/g of the ZT0.02 composite electrode.

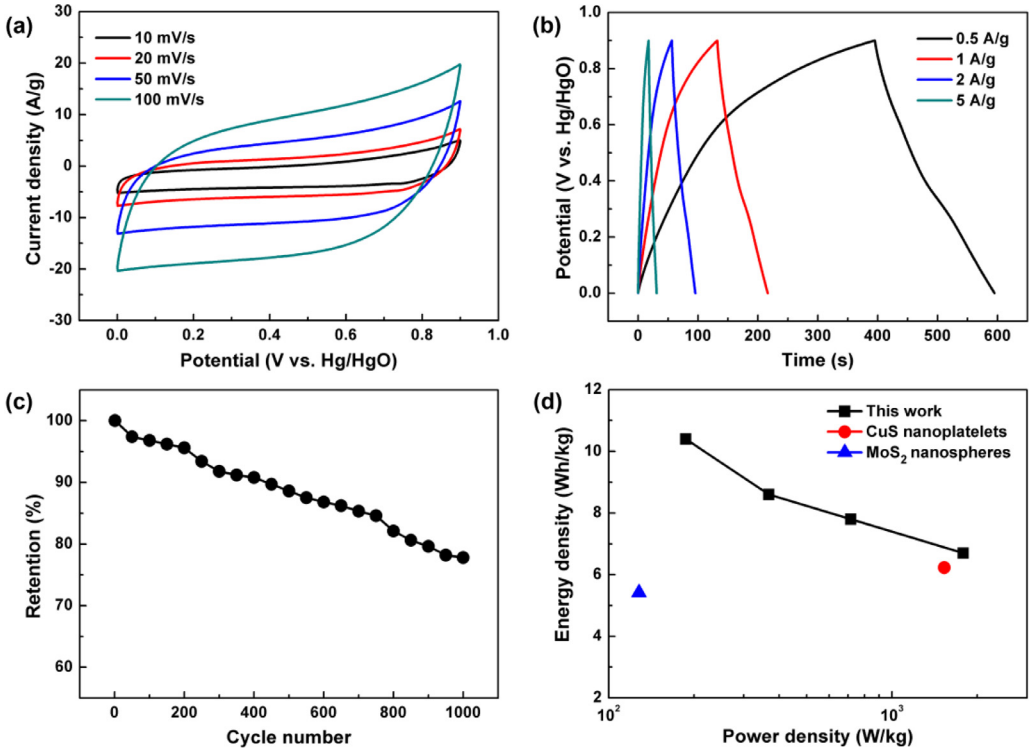

Fig. 5. (a) CV curves at different scan rates, (b) GCD curves at different current densities, (c) cycle performance at a current density of 5 A/g, and (d) Ragone plots of symmetric g-C_3N_4/ZnS//g-C_3N_4/ZnS cell.

higher than those of pure g-C_3N_4 and its composites (see Table 2), and ZnS (11.3 F/g at 0.5 A/g) [13]. Obviously, the specific capacitance of the ZT0.02 composite electrode still remains as high as 349.7 F/g even at a high current density of 10 A/g, which remains 70.2% of the initial value at 1 A/g. The decrease in specific capacitance at high current density is attributed to the resistance of the electrode and the insufficient Faradaic redox reaction of active materials [24]. The cycling stability of the ZT0.02 composite electrode is also shown in Fig. 4(d). It can be seen that the ZT0.02 composite electrode exhibits a 20% loss of the initial specific capacitance at 5 A/g after 1000 charge-discharge cycles, indicating a good cycling stability.

Table 2. Performance comparisons of the present work with other electrode materials based g-C_3N_4 and its composites.

Electrode	Specific capacitance	Cycling performance	Refs.
ZnS/g-C_3N_4	497.7 F/g at 1 A/g	80.4% after 1000 cycles at 5 A/g	This work
g-C_3N_4 nanofibers	263.8 F/g at 1 A/g	93.6% after 2000 cycles at 1 A/g	[20]
Tubular g-C_3N_4	233 F/g at 0.2 A/g	90% after 1000 cycles at 0.2 A/g	[37]
$Ni(OH)_2$/g-C_3N_4	445.6 F/g at 1 A/g	71.5% after 1000 cycles	[38]
MnO_2/g-C_3N_4	211 F/g at 1 A/g	Unchanged after 1000 cycles at 2 A/g	[39]
α-Fe_2O_3/g-C_3N_4	167 F/g at 1 A/g	Remarkable long-term cycling stability	[40]
Fe_3O_4/g-C_3N_4	56.7 F/g at 1 A/g		[41]

To further explore the feasibility of g-C_3N_4/ZnS composite electrodes for practical application, we developed a symmetric supercapacitor device by clamping together two pieces of g-C_3N_4/ZnS composite electrodes separated by a polymer filtering membrane (Celgrad 3501) in 6 M KOH aqueous electrolyte. Fig. 5(a) shows the CV curves of the symmetric supercapacitor device at different scan rates. The increase of current density with respect to the increase in scan rate can be seen. Moreover, the shapes of CV curves show no obvious changes even at higher scan rate, indicating good rate capability. The cell capacitances of the symmetric supercapacitor device at various current densities are calculated from the GCD curves (Fig. 5b). The symmetric supercapacitor device achieves a high capacitance of 92.8 F/g at a current density of 0.5 A/g and can still maintain 59.2 F/g even at a high current density of 5 A/g, holding a capacitance retention of 63.8%. The cycling performance of the symmetric supercapacitor device is evaluated by GCD test at a current density of 5 A/g, as presented in Fig. 5(c). After 1000 cycles, the cell capacitance can retain 77.8% of the initial value. Fig. 5(d) shows the comparison of the relationship between power density and energy density of the symmetric supercapacitor device to other metal sulfides. A high energy density of 10.4 Wh/kg is obtained from the symmetric supercapacitor device at a power density of 187.3 W/kg, which is not outstanding but exceeds those of most metal sulfides, such as MoS_2 nanospheres and CuS nanoplatelets [42,43].

4. Conclusions

In summary, we have synthesized a series of g-C_3N_4/ZnS composites using a feasible controlled one-step calcination method. A specific capacitance of 497.7 F/g at 1 A/g, with good rate capability (70.2% retention from 1 A/g to 10 A/g) and excellent cycling stability (80.4% retention at 5 A/g after 1000 cycles), is achieved for the final obtained g-C_3N_4/ZnS composite electrode in 6 M KOH aqueous electrolyte. In addition, g-C_3N_4/ZnS composite electrodes deliver an enhanced supercapacitor performance compared to the pristine g-C_3N_4 and ZnS. Furthermore, the symmetric supercapacitor device assembled from two pieces of g-C_3N_4/ZnS composite electrodes shows a high energy density of 10.4 Wh/kg at a power density of 187.3 W/kg. These results suggest that g-C_3N_4/ZnS composites can be used as electrode materials for supercapacitor applications.

Acknowledgments

This work was supported by the National Nature Science Foundations of China (Grant no. 51372212).

References

[1] H. Heydari, S.E. Moosavifard, M. Shahraki, S. Elyasi, J. Energy Chem. 26 (2017) 762–767.
[2] Q. Cheng, J. Tang, N. Shinya, L.C. Qin, J. Power Sources 241 (2013) 423–428.
[3] V.H. Nguyen, J.J. Shim, J. Power Sources 273 (2015) 110–117.
[4] G.H. Yu, L.B. Hu, N. Liu, H.L. Wang, M. Vosgueritchian, Y. Yang, Y. Cui, Z.N. Bao, Nano Lett. 11 (2011) 4438–4442.
[5] L.L. Zhang, X.S. Zhao, Chem. Soc. Rev. 38 (2009) 2520–2531.
[6] J. Pu, Z.H. Wang, K.L. Wu, N. Yu, E. Sheng, Phys. Chem. Chem. Phys. 16 (2014) 785–791.
[7] V. Gupta, T. Kusahara, H. Toyama, S. Gupta, N. Miura, Electrochem. Commun. 9 (2007) 2315–2319.
[8] C.C. Hu, K.H. Chang, M.C. Lin, Y.T. Wu, Nano Lett. 6 (2006) 2690–2695.
[9] H.C. Gao, F. Xiao, C.B. Ching, H.W. Duan, ACS Appl. Mater. Interface 4 (2012) 2801–2810.
[10] C.J. Raj, B.C. Kim, W.J. Cho, W.G. Lee, Y. Seo, K.H. Yu, J. Alloys Compd. 586 (2014) 191–196.
[11] Y. Li, H.Q. Xie, J.P. Tu, Mater. Lett. 63 (2009) 1785–1787.
[12] K. Krishnamoorthy, G.K. Veerasubramani, S. Radhakrishnan, S.J. Kim, Chem. Eng. J. 251 (2014) 116–122.
[13] R. Ramachandran, M. Saranya, P. Kollu, B.P.C. Raghupathy, S.K. Jeong, A.N. Grace, Electrochim. Acta 178 (2015) 647–657.
[14] M. Jayalakshmi, M.M. Rao, J. Power Sources 157 (2006) 624–629.
[15] M.S. Javed, J. Chen, L. Chen, Y. Xi, C.L. Zhang, B.Y. Wan, C.G. Hu, J. Mater. Chem. A 4 (2016) 667–674.
[16] G.C. Li, M.M. Liu, M.K. Wu, P.F. Liu, Z.W. Zhou, S.R. Zhu, R. Liu, L. Han, RSC Adv. 6 (2016) 103517–103522.
[17] G.P. Dong, Y.H. Zhang, Q.W. Pan, J.R. Qiu, J. Photochem. Photobiol. C 20 (2014) 33–50.
[18] D.J. Martin, K.P. Qiu, S.A. Shevlin, A.D. Handoko, X.W. Chen, Z.X. Guo, J.W. Tang, Angew. Chem. Int. Ed. 53 (2014) 9240–9245.
[19] Q. Liu, J.Y. Zhang, Langmuir 29 (2013) 3821–3828.
[20] M. Tahir, C.B. Cao, N. Mahmood, F.K. Butt, A. Mahmood, F. Idrees, S. Hussain, M. Tanveer, Z. Ali, I. Aslam, ACS Appl. Mater. Interface 6 (2014) 1258–1265.
[21] Y. Zhang, R.Y. Wen, D. Guo, H.X. Guo, J.H. Chen, Z.S. Zheng, Appl. Organomet. Chem. 30 (2016) 160–166.
[22] P. Suyana, K.R. Sneha, B.N. Nair, V. Karunakaran, A.P. Mohamed, K.G.K. Warrier, U.S. Hareesh, RSC Adv. 6 (2016) 17800–17809.
[23] Q.Z. Wang, Y.B. Shi, Z.Y. Du, J.J. He, J.B. Zhong, L.C. Zhao, H.D. She, G. Liu, B.T. Su, Eur. J. Inorg. Chem. 24 (2015) 4108–4115.
[24] K.J. Huang, J.Z. Zhang, K. Xing, Electrochim. Acta 149 (2014) 28–33.
[25] F. He, G. Chen, Y.G. Yu, Y.S. Zhou, Y. Zheng, S. Hao, Chem. Commun. 51 (2015) 425–427.
[26] L. Ge, F. Zuo, J.K. Liu, Q. Ma, C. Wang, D.Z. Sun, L. Bartels, P.Y. Feng, J. Phys. Chem. C 25 (2012) 13708–13714.
[27] W.J. Ong, L.L. Tan, S.P. Chai, S.T. Yong, Dalton Trans. 44 (2015) 1249–1257.
[28] J. Hou, T.Y. Zhou, L. Wang, P. Zhang, L.Ding, Sens. Actuators, B 230 (2016) 615–622.
[29] F.F. Shi, L.L. Chen, C.S. Xing, D.L. Jiang, D. Li, M. Chen, RSC Adv. 4 (2014) 62223–62229.
[30] X.H. Lu, D.Z. Zheng, T. Zhai, Z.Q. Liu, Y.Y. Huang, S.L. Xie, Y.X. Tong, Energy Environ. Sci. 4 (2011) 2915–2921.
[31] D.L. Jiang, Q. Xu, S.C. Meng, C.K. Xia, M. Chen, J. Alloys Compd 706 (2017) 41–47.
[32] J. Pu, F.L. Cui, S.B. Chu, T.T. Wang, E.H. Sheng, Z.H. Wang, ACS Sustainable Chem. Eng. 2 (2014) 809–815.
[33] J.W. Zhu, S. Chen, H. Zhou, X. Wang, Nano Res. 5 (2012) 11–19.
[34] J.W. Lee, J.M. Ko, J.D. Kim, Electrochim. Acta 85 (2012) 459–466.
[35] K.J. Huang, J.Z. Zhang, J.L. Cai, Electrochim. Acta 180 (2015) 770–777.
[36] X. Liu, J.Z. Zhang, K.J. Huang, P. Hao, Chem. Eng. J. 302 (2016) 437–445.
[37] M. Tahir, C.B. Cao, F.K. Butt, F. Idrees, N. Mahmood, Z. Ali, I. Aslam, M. Tanveer, M. Rizwan, T. Mahmood, J. Mater. Chem. A 1 (2013) 13949–13955.
[38] L. Shi, J.L. Zhang, H.D. Liu, M.N. Que, X. Cai, S.Z. Tan, L.H. Huang, Mater. Lett. 145 (2015) 150–153.
[39] X.T. Chang, X.X. Zhai, S.B. Sun, D.X. Gu, L.H. Dong, Y.S. Yin, Y.Q. Zhu, Nanotechnology 28 (2017) 135705.
[40] L. Xu, J.X. Xia, H. Xu, S. Yin, K. Wang, L.Y. Huang, L.G. Wang, H.M. Li, J. Power Sources 245 (2014) 866–874.
[41] Y.Z. Wu, M. Chen, X.H. Yan, J. Ren, Y. Dai, J.J. Wang, J.M. Pan, Y.P. Wang, X.N. Cheng, Mater. Lett. 198 (2017) 114–117.
[42] M.S. Javed, S. Dai, M.J. Wang, D.L. Guo, L. Chen, X. Wang, C.G. Hu, Y. Xi, J. Power Sources 285 (2015) 63–69.
[43] C.J. Raj, B.C. Kim, W.J. Cho, W.G. Lee, Y. Seo, K.H. Yu, J. Alloys Compd. 586 (2014) 191–196.